ADVANCED FUNCTIONAL MATERIALS
www.afm-journal.de

In-Liquid Plasma for Surface Engineering of Cu Electrodes with Incorporated SiO_2 Nanoparticles: From Micro to Nano

*Pramod V. Menezes, Mohamed M. Elnagar, Mohammad Al-Shakran, Maximilian J. Eckl, Prashanth W. Menezes, Ludwig A. Kibler, and Timo Jacob**

A robust and efficient route to modify the chemical and physical properties of polycrystalline copper (Cu) wires via versatile plasma electrolysis is presented. Silica (SiO_2) nanoparticles (11 nm) are introduced during the electrolysis to tailor the surface structure of the Cu electrode. The influence of these SiO_2 nanoparticles on the structure of the Cu electrodes during plasma electrolysis over a wide array of applied voltages and processing time is investigated systematically. Homogeneously distributed 3D coral-like microstructures are observed by scanning electron microscopy on the Cu surface after the in-liquid plasma treatment. These 3D microstructures grow with increasing plasma processing time. Interestingly, the microstructured copper electrode is composed of CuO as a thin outer layer and a significant amount of inner Cu_2O. Furthermore, the oxide film thickness (between 1 and 70 µm), the surface morphology, and the chemical composition can be tuned by controlling the plasma parameters. Remarkably, the fabricated microstructures can be transformed to nanospheres assembled in coral-like microstructures by a simple electrochemical treatment.

1. Introduction

Conversion reactions that turn simple and abundant base molecules, particularly carbon dioxide (CO_2), water, and molecular nitrogen into valuable and industrially relevant chemicals, have been subject of extensive research. Presently, these fascinating reactions are indispensable in modern electrochemistry-related technologies such as fuel cells, water splitting, energy storage devices, electroreduction of CO_2 (CO_2RR) to hydrocarbons, and many more.[1–3] A crucial aspect in this regard is the design of electrocatalysts that fulfill the requirements of high performance and selectivity, operating at low applied overpotentials, minor parasitic reactions, and long-term stability.[4,5] Moreover, tremendous efforts are devoted to substituting precious metal electrocatalysts with earth-abundant metals of comparable catalytic activity. From this perspective, copper (Cu)-based materials have emerged as one of the most auspicious candidates especially in the field of electrocatalysis.[6–9] For instance, Cu is the only metal that has exhibited a propensity for CO_2RR to $>2e^-$ products at significant rates and selectivity due to its negative adsorption energy for carbon monoxide (an essential CO_2RR intermediate) and positive adsorption energy for hydrogen (an intermediate in the competitive hydrogen evolution reaction).[7,10–12] Furthermore, Cu-based electrodes have shown high activity towards oxygen evolution reaction (OER), hydrogen evolution reaction (HER) as well as overall water splitting at different pH values.[13–15]

The catalytic activity and selectivity, as well as reaction mechanisms of Cu-based materials are rather dependent on the surface morphology, surface structure (roughness, grain boundaries, crystal facets, defects, and heteroatom doping), and chemical state (subsurface oxygen and Cu(I) species).[16–20] Hence, controlling these properties based on materials design principles derived from deep mechanistic understanding and surface structure–performance relations can guide the activity and selectivity of Cu-based electrocatalysts.[6,21] For this purpose, micro and nanostructured Cu catalysts are of special consideration owing to their superior selectivity and performance for several electrocatalytic reactions.[6,9,22–25]

Commonly, the micro and nanostructured Cu-based materials with controlled particle size, chemical composition, and surface morphology are synthesized by solid-state or solution-based techniques.[26–28] Most of these methods involve organic surfactants

P. V. Menezes, M. M. Elnagar, M. Al-Shakran, M. J. Eckl, L. A. Kibler, T. Jacob
Institute of Electrochemistry
Ulm University
89081 Ulm, Germany
E-mail: timo.jacob@uni-ulm.de
P. W. Menezes
Institute of Chemistry
Technical University of Berlin
10623 Berlin, Germany
P. W. Menezes
Materials Chemistry Group for Thin Film Catalysis – CatLab
Helmholtz-Zentrum Berlin für Materialien und Energie
Albert-Einstein-Str. 15, 12489 Berlin, Germany
T. Jacob
Helmholtz-Institute-Ulm (HIU) Electrochemical Energy Storage
89081 Ulm, Germany
T. Jacob
Karlsruhe Institute of Technology (KIT)
P.O. Box 3640, 76021 Karlsruhe, Germany

The ORCID identification number(s) for the author(s) of this article can be found under https://doi.org/10.1002/adfm.202107058.

DOI: 10.1002/adfm.202107058

as structure-directing agents which can modify, even mask, the surface chemistry of the micro and nanostructures. Moreover, electrodes of these materials can be fabricated by deposition onto suitable support in the presence of polymeric binders (e.g., Nafion or polytetrafluoroethylene). However, under electrochemical operating conditions, these electrodes suffer from several drawbacks including mechanical instability of the micro/nanostructures due to binder decomposition, lower electrical conductivity, deactivation due to masking of the active catalytic sites, and structural transformations.[29,30] In contrast, electrochemical approaches afford an alternative route for tailoring the electrode surface structure.[31–35]

More specifically, self-organization and self-assembly processes at the exposed metal surface induced by surface stress are very effective strategies to facilitate the fabrication of unique micro/nanostructures and metamaterials.[36–39] In other words, the application of a self-organization tool to fabricate micro- and nanostructures allows controlling the growth of a defined crystalline structure, chemical composition, and the specific surface area of the obtained materials. Nevertheless, inducing and controlling the self-organization processes is not a straightforward task since they frequently arise from a complex interplay of physical and chemical processes.[39]

In this context, plasma electrolysis (PE) is considered a versatile and green approach that enables electric field-driven controlled self-organization and self-assembly over a wide spectrum of length scales from micro- to nanometers.[36,40–42] Consequently, in-liquid plasma can be effectively used for the formation of large arrays of tailored micro/nanostructures and surface functionalization depending on the experimental conditions such as the electrolyte composition, electrode material, applied voltage, and more.[43–47] In plasma electrolytic oxidation, the electrolyte supplies high electrical conductivity and induces a particular anodization reaction at the anode surface to grow its oxide or hydroxide film with a definite morphology.[43,46–48]

Previous studies have shown that foreign atoms can remarkably affect the structural and chemical properties of anodized films as well as the plasma operating parameters.[49,50] Particle addition such as SiO_2, Si_3N_4, TiO_2, Al_2O_2, ZrO_2, Ag, CeO_2, etc. into the alkaline electrolyte and their incorporation mode with the substrate (Al, Mg, Ti, and their alloys) turned out to be useful for the fabrication of new materials with altered chemical compositions and functionalities.[43,49,51–53] Interestingly, previous studies reveal that the interface between silica and the catalyst can actively participate in the reaction.[54–56] For instance, the incorporation of SiO_2 into the Cu surface induces outstanding effects such as promoting catalytic hydrogenation of esters and improving the cycle performance of the cells for high-performance lithium-ion batteries.[54,57]

In this study, we present a rapid, green, and facile one-step fabrication of microstructured Cu-based electrodes via a plasma electrolysis approach using a sacrificial SiO_2 nanoparticles template. We chose a wire-type electrode as a substrate due to its flexibility and widespread applications in energy technologies. Changes in the surface structure, chemical composition, and electrochemical behavior of the Cu electrodes as a function of applied voltage and treatment time as well as upon the addition of SiO_2 nanoparticles were systematically investigated. Interestingly, plasma electrolysis in the presence of SiO_2 nanoparticles enables self-organization and self-assembly at the plasma–Cu interfaces to produce homogenous 3D coral-like microstructures. This microstructured Cu electrode is mainly composed of a significant amount of Cu_2O as the inner layer and a thin outer layer (shell) of CuO, besides a minor amount of homogenously distributed SiO_2. More importantly, the film thickness (ranging from 1 to 70 μm), surface morphology, chemical composition, and surface roughness can be tuned by controlling the plasma parameters. Moreover, potential cycling of the coral-like microstructured Cu electrodes in 0.1 M potassium hydroxide (KOH) solution induces a remarkable structural transformation from bulk coral-like microstructures to nanospheres, but still assembled in coral-like micropatterns.

2. Results and Discussion

2.1. Effect of SiO_2 Nanoparticles on Plasma Electrolysis

The plasma electrolysis of Cu anodes was carried out through a simple asymmetric two-electrode system, as schematically shown in **Figure 1**a. Details on the experimental setup are provided in the Experimental Section. To study the influence of the presence of SiO_2 nanoparticles during plasma electrolysis on the surface structure of the Cu electrodes, we compared the results obtained after plasma electrolysis in either 0.01 M KOH or 0.01 M KOH + 0.001 M SiO_2 (particle size 11 nm). SEM micrographs of the Cu surface before and after plasma electrolysis in both electrolytes at 525 V for 60 s are given in Figure 1b–e. In contrast to the as-polished wire (Figure 1b), anodic polarization of the Cu electrode in both electrolytes alters the surface structure remarkably, but one could observe significant morphological differences depending on the electrolyte composition (Figure 1c,e). The surface of the Cu electrode treated in the KOH electrolyte is covered with a dimpled structure, as shown in Figure 1c. Such structures might be formed due to the steam corrosion of Cu at a high temperature and subsequent reaction with the hydroxide ions of the electrolyte during plasma electrolysis.[58] Furthermore, the huge amount of gas bubbles generated on the surface process affects the final surface morphology.[48] Interestingly, the addition of SiO_2 to the electrolyte enables self-organization and self-assembly at the plasma/Cu interfaces, inducing the formation of homogenously distributed 3D coral-like microstructures on the surface of the polarized Cu electrode (Figure 1d,e). In this sense, the manifest impact of SiO_2 nanoparticles on the surface morphology of Cu surface indicates the active incorporation of SiO_2 nanoparticles into the Cu surface during plasma electrolysis. One should emphasize that the silica particle size must be in the nanometer regime to achieve active incorporation.[49,50] The feasibility for microparticles to transform to a new phase through plasma discharge is considerably lower than that for the nanoparticles except for the particles with a low melting point.[50] In this respect, large-sized SiO_2 particles typically show inactive incorporation, as the short-lived discharges cannot melt these particles completely.[49] Therefore, SiO_2 with a mean particle size of 11 nm was selected in this study. Yet, the nanoparticles need an external force to be delivered to the electrolyte/metal interface for participating in the plasma electrolysis. After the dispersion of SiO_2 nanoparticles in the KOH electrolyte and their interaction with hydroxide ions, the particles will become negatively charged.[49,59] Afterward, these particles migrate toward the Cu anode due to the applied high electric field and ultimately generating self-organization across various levels and spatial scales.

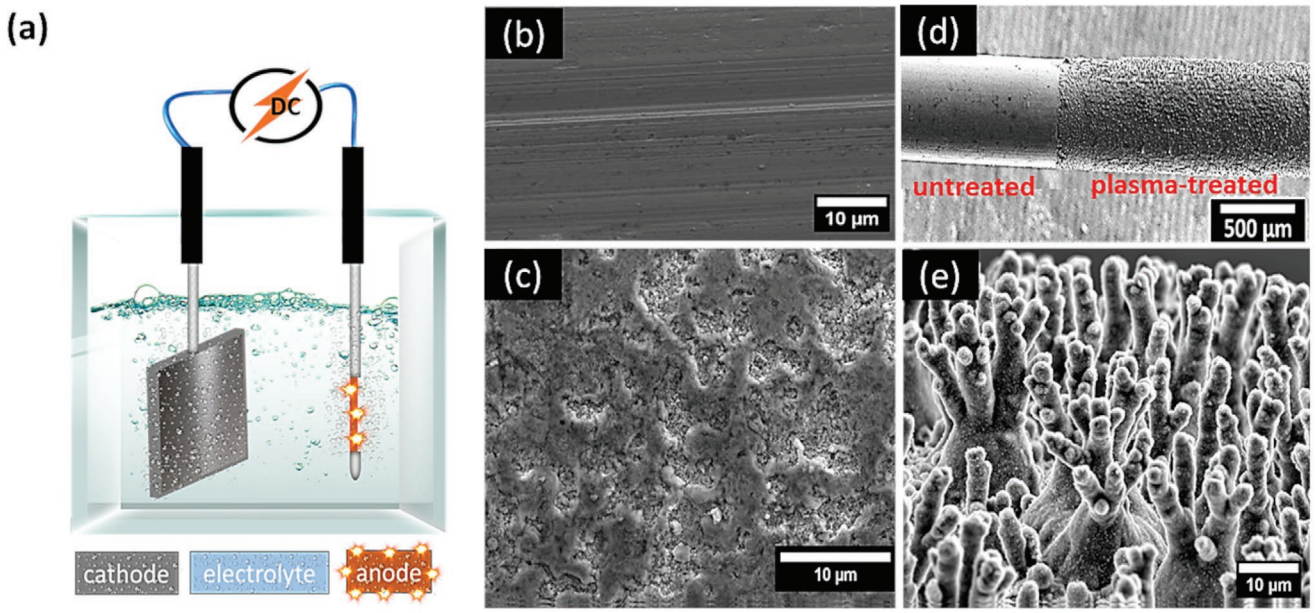

Figure 1. a) Schematic illustration of a two-electrode plasma electrolysis system. SEM micrographs of b) the as-polished Cu surface and after polarization at 525 V for 60 s in c) 0.01 M KOH, and d,e) in 0.01 M KOH + 0.001 M SiO_2.

Furthermore, SiO_2 readily creates highly active interfaces with Cu under plasma conditions and serves as a sacrificial nanoparticle template resulting in the growth of 3D coral-like microstructures.[54,60] Such specific surface structure might be driven by the innate propensity of the system to reach a local energy minimum.

2.2. *j–U* Characteristics

Figure 2a compares the stationary current density–voltage (*j–U*) characteristics of the Cu wire electrodes recorded for 60 s electrolysis in either 0.01 M KOH or 0.01 M KOH + 0.001 M SiO_2. The average current values over a wide array of voltages (50–600 V) are measured with freshly prepared electrodes and electrolytes for each voltage as well as the initial temperature of the electrolyte was kept at 30 °C.

Based on the obtained results, the *j–U* characteristics are divided into four different stages; stage A (50–350 V), stage B (400 V), stage C (400–500 V), and stage D (500–600 V).[61–63] In stage A, the current density increases as a function of the applied voltage, which complies with Ohm's law and Faraday's law of electrolysis. During this stage, the evolution of the gaseous envelope was observed around the electrode/electrolyte interface, and the intensity of the gaseous envelope gradually increased with increasing the voltage, as shown in Figure 2b. At the peak of the *j–U* curve (stage B, breakdown voltage region), the continuous gaseous envelope covers the whole surface of the electrode, which leads to low electrical conductivity. As a result, the current drops at stage C (400–500 V), due to the high electrical resistance of the gaseous envelopes and unstable region between electrode/electrolyte interface. At the beginning of stage D, numerous small micro-plasma discharges start to spread out homogeneously on the electrode surface, as illustrated in Figure 2b. Then, the intensity of these plasma emissions significantly increases with increasing the voltage, thus the current decreases to the lowest point at 575 V and then slightly increases with increasing the applied voltage to 600 V. The plasma regime is highlighted in red colored circles. Going beyond 600 V results in a large emission of plasmas accompanied by melting of the wire as shown in Figure 2b (625 V) due to the extreme plasma heat. Figure 2b shows that the Cu surface turned black after applying a voltage within a few seconds,

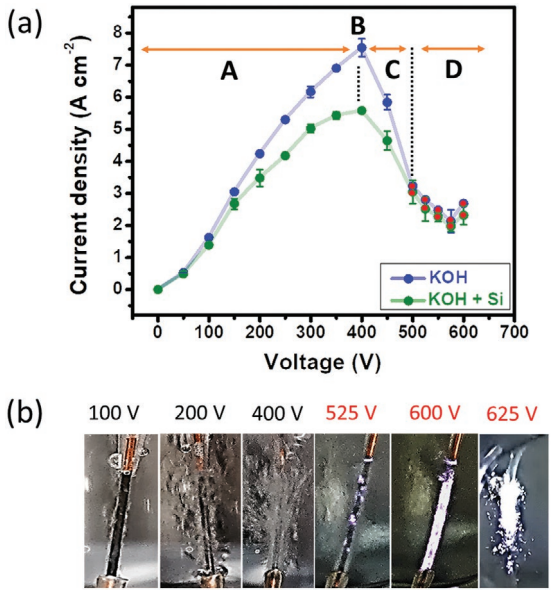

Figure 2. a) Current density versus voltage during the electrolysis of a Cu electrode in 0.01 M KOH (blue) or 0.01 M KOH + 0.001 M SiO_2 (green). b) Optical graphs of the Cu wire during electrolysis at different voltages in 0.01 M KOH + 0.001 M SiO_2 electrolyte.

which reveals the formation of CuO. It is obvious that the addition of SiO_2 nanoparticles considerably affects the evolution of the current during the whole process. Under the constant voltage mode, current density decreases in the presence of SiO_2 nanoparticles compared to the 0.01 M KOH electrolyte. This implies the formation of a thicker and denser isolating film and an increase in impedance driven by the addition of SiO_2 nanoparticles.

2.3. Surface Characterization

We systematically investigated the evolution of the Cu surface morphology and composition after an anodic polarization of 60 s in either 0.01 M KOH + 0.001 M SiO_2 or 0.01 M KOH electrolytes as a function of the applied voltage (50–600 V). The corresponding SEM micrographs and EDS analyses are presented in **Figure 3** and Figure S1, Supporting Information, respectively. As shown in Figure 2a,b, applying voltages in the range of 100 V ≤ U < 300 V leads to a rough surface, dominated by the formation of flake-like structures. Despite the EDS analysis (Figure 3i) for these electrodes revealing the presence of Si (<10%), similar surface features are also observed for the Cu electrodes treated in 0.01 M KOH at the same voltage, as shown in Figure S1a, Supporting Information. These observations indicate the inactive incorporation of SiO_2 nanoparticles at these voltages.[49,50] In comparison, after polarization at 300 V, the SiO_2 nanoparticles actively interact with the Cu surface producing oxide composed coral seeds. The density of the coral seeds is sustainably increased with increasing the applied voltage to 400 V (Figure 3d). Remarkably, applying voltages in the plasma regime, 500 V ≤ U ≤ 550 V, induces the growth of 3D coral-like microstructures from the coral seeds, as shown in Figure 3e,f. These microstructures contain a high content of O (≈55%) and Cu (≈38%), besides a small amount of Si (<10%), as determined by EDS elemental mapping (Figure 3i). Furthermore, Figure 3j demonstrates that Si is distributed homogeneously over the coral surface. These findings reveal the active incorporation of SiO_2 nanoparticles at sufficiently high voltages. Normally, active incorporation is attainable when the particles melt through high-energy discharges, and then they can interact with the electrode.[49,50,64] Further increase of the applied voltage to 575 V results in a pronounced dissolution of the 3D coral-like

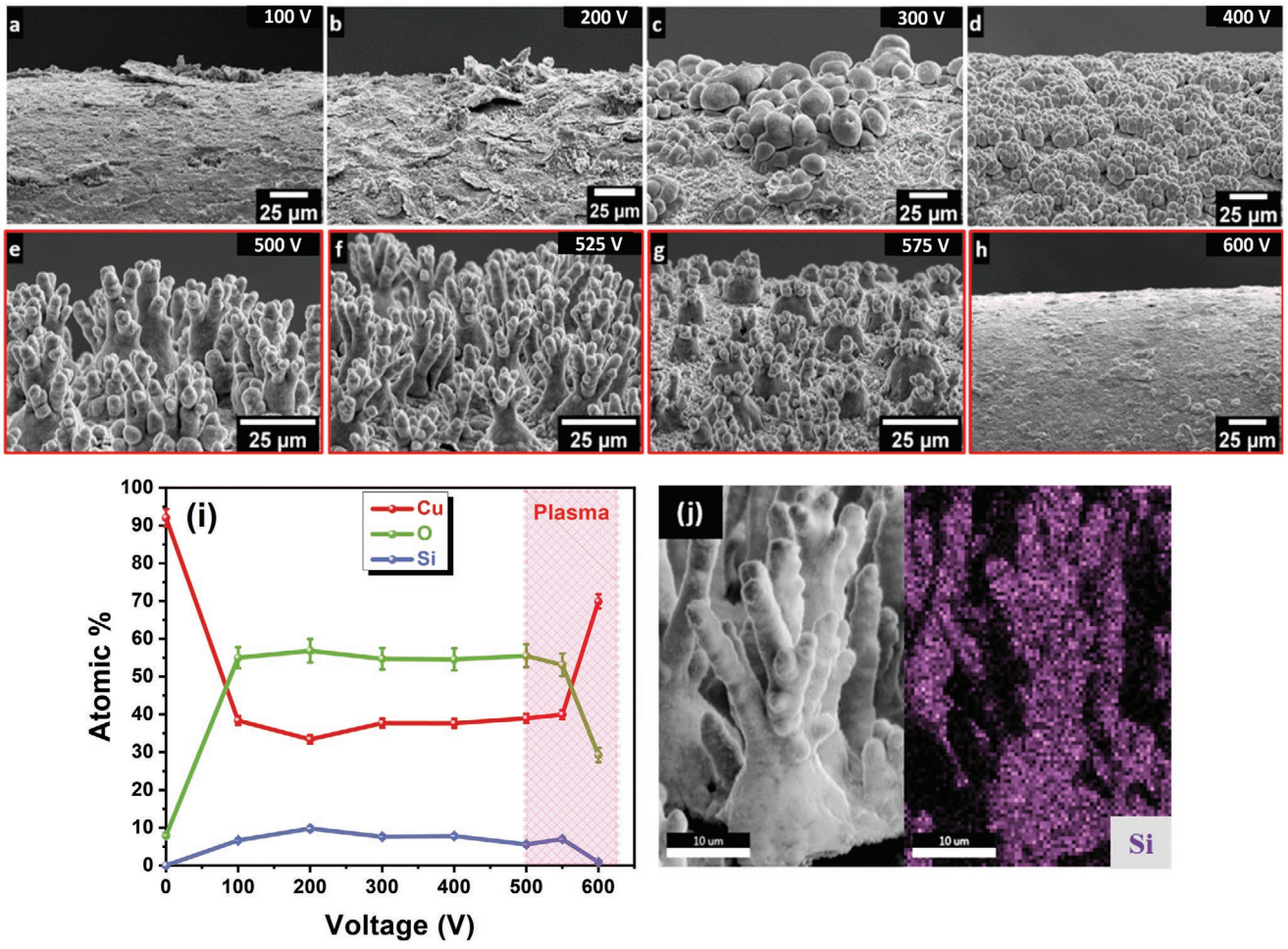

Figure 3. a–h) SEM micrographs of Cu electrodes treated in 0.01 M KOH + 0.001 M SiO_2 electrolyte for 60 s as a function of the applied voltages. i) Their corresponding elemental compositions were determined by EDS analysis. The error bars represent the deviation range of EDS measurements. The surface morphology of Cu electrodes treated in the plasma regime is red-rimmed. j) EDS elemental mapping for Si distribution over the 3D coral-like microstructures and the corresponding SEM micrograph.

microstructures (Figure 3g). Moreover, a smoother surface with the absence of the 3D coral-like microstructures is observed after polarization at $U \geq 600$ V (Figure 3h), which is attributed to the extreme plasma discharge as indicated in Figure 2. Notably, at these voltage ranges, the amount of surface oxygen considerably decreases and there is no incorporation of SiO_2 nanoparticles since Si cannot be detected on the Cu surface, as indicated by EDS analysis (see Figure 3i). During polarization at 600 V, the oxide layer is partly removed which might be due to the bubble implosion induced by the extreme plasma discharge. Furthermore, plasma electrolysis at these extreme voltages is accompanied by the formation of reducing species (e.g., H_2O_2) and massive hydrogen evolution that could chemically reduce CuO.[65,66]

In comparison, after polarization of Cu electrodes solely in 0.01 M KOH electrolyte at voltages in the range of $50 \text{ V} \leq U < 500$ V, a thick oxide layer forms on their surfaces as indicated by 50% of O (Figure S1b, Supporting Information). Moreover, for the plasma regime (500–600 V), the thickness of the surface oxide layer decreases drastically, and the surface becomes smoother, as indicated by the SEM and EDS results in Figures S1a,b, Supporting Information.

Figure 4 presents SEM micrographs of the Cu electrode after plasma electrolysis at 525 V in 0.01 M KOH + 0.001 M SiO_2 for various polarization times ranging from 15 to 1800 s. Since the 3D coral-like microstructures are observed after applying voltages in the range of $500 \text{ V} \leq U \leq 550$ V, we investigated the

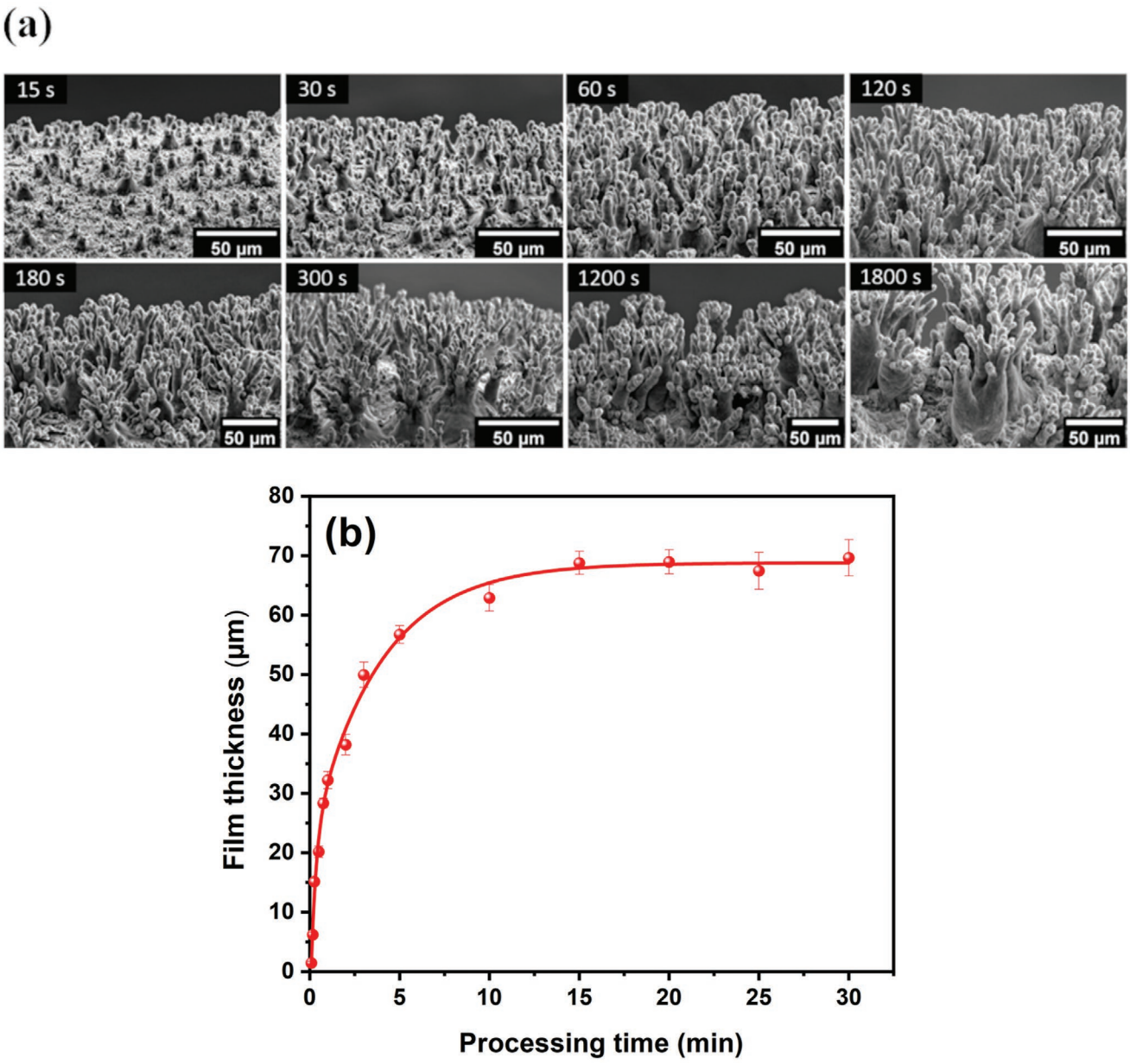

Figure 4. a) Evolution of surface morphology upon plasma treatment at 525 V for various polarization times as illustrated by SEM images of Cu electrode after 15, 30, 60, 120, 180, 300, 1200, and 1800 s. b) The thickness of the coral film as a function of plasma treatment time.

effect of polarization time at 525 V. The Cu polarized at 525 V as a prototype was selected for further investigations.

SEM imaging of the Cu electrode for increasing polarization times demonstrates the continuous development of the 3D coral-like microstructures. Consequently, the film thickness was estimated from the SEM images by measuring the coral height from bottom to top at different plasma treatment times. As shown in Figure 4b, the development of the coral height increases rapidly at the beginning of the processing time till 10 min. Then, the growth rate gradually reduces with increasing treatment time up to 15 min, after which there is almost no further development up to 30 min. This trend could be attributed to the increase of local temperature at the electrode surface during the continuous plasma processing time, which affects the plasma conditions such as cell current density.[46,67,68] The significant drop of the growth rate at a certain distance from the electrode is due to diffusion limitation. At higher temperatures, the reaction kinetics considerably increase inducing a faster reaction of the formed Cu ions. One should notice that the thickness of the diffusion layer is influenced by various factors (e.g., convection) that are not yet well understood, especially under the extreme conditions of plasma electrolysis.

The EDS analysis implies that the ratios of Cu, O, and Si in the 3D coral-like microstructures are almost identical in the bulk and near the surface for all treated Cu samples as a function of treatment time, as shown in Figure S2, Supporting Information.

To gain deeper insights into the internal structure and chemical composition of the 3D coral-like microstructure, a focused ion beam scanning electron microscopy (FIB-SEM) system coupled with energy-dispersive X-ray spectroscopy (EDS) was utilized. For this reason, we selected the Cu electrode with well-defined and homogenously distributed 3D coral-like microstructures which form at 525 V during 60 s. The cross-section of the upper part (green-highlighted in **Figure 5**a) reveals that the internal structure of the coral branches is porous with a shell thickness of roughly 2 µm, as presented in Figure 5b. EDS point analysis on the coral surface, the inner porous layer, and the coral shell surface illustrates comparable contents of Cu, O, and Si for these three regions, as determined in the green, blue, and orange tables, respectively. Additionally, Figure 5c shows the SEM image of the cross-sectioned bottom part of the coral (red-highlighted in Figure 5a), which was prepared by milling away layers of ≈4 µm thickness using the gallium ion beam. A porous oxide surface is observed at 4 µm depth which contains ≈9.5% of Si, as shown in Figure 5c and its related yellow table. Due to the complexity of the coral-like structure and its analysis, we add another example for the FIB–SEM cross-section and EDS point analysis of the coral surface is presented in Figure S3, Supporting Information.

XPS analysis was conducted to identify changes in the chemical composition and oxidation state of Cu species of the topmost oxide layer after plasma treatment in 0.01 M KOH + 0.001 M SiO_2 at 525 V for various treatment times. Figure S4, Supporting Information, compares the whole XPS spectra (survey) of the as-polished Cu electrode and the 30, 60, 180, and 300 s plasma-treated Cu electrodes. From the survey spectra, the peaks corresponding to Cu, O, C, and Si are detected. The high-resolution spectra (core level) of Cu 2*p* for the as-polished Cu electrode and the plasma-modified electrodes are shown in **Figure 6**a. The Cu $2p_{3/2}$ binding energy (BE) is 933.6 eV for Cu(II)O and 932.4 eV for Cu(I)O/metallic Cu (note that the Cu 2*p* binding energies of Cu(I) and Cu(0) species are very close).[69,70] Based on the obtained spectra, we can confirm that the as-polished Cu electrode is composed of Cu(II)O and Cu(I)O/Cu(0). In comparison, Cu(II)O is detected in the spectra of the plasma-treated electrodes independent of the processing time, as shown in Figure 6a. To further investigate the oxidation states of the plasma-modified Cu electrode, an XPS depth profiling measurement was performed with different sputter depth rates of 3, 10, and 30 nm min^{-1} for the samples treated at 525 V for 60 s, as demonstrated in

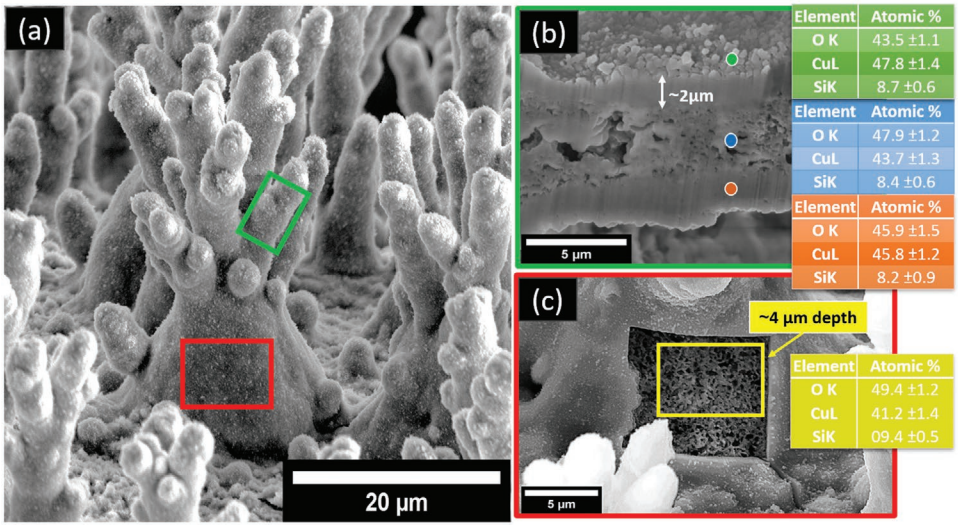

Figure 5. FIB–SEM cross-section of the 3D coral-like structure and the EDS analysis. a) SEM image of the 3D coral-like microstructures where the cross-section regions are indicated in green and red color. b) SEM image of the cross-sectioned coral branches that reveals the coral shell thickness of ≈2 µm, and the three different EDS analysis regions indicated in green, blue, and orange colors. c) SEM image of the cross-sectioned coral-like structure, which was obtained by milling away of ≈4 µm from the surface and corresponding EDS analysis data.

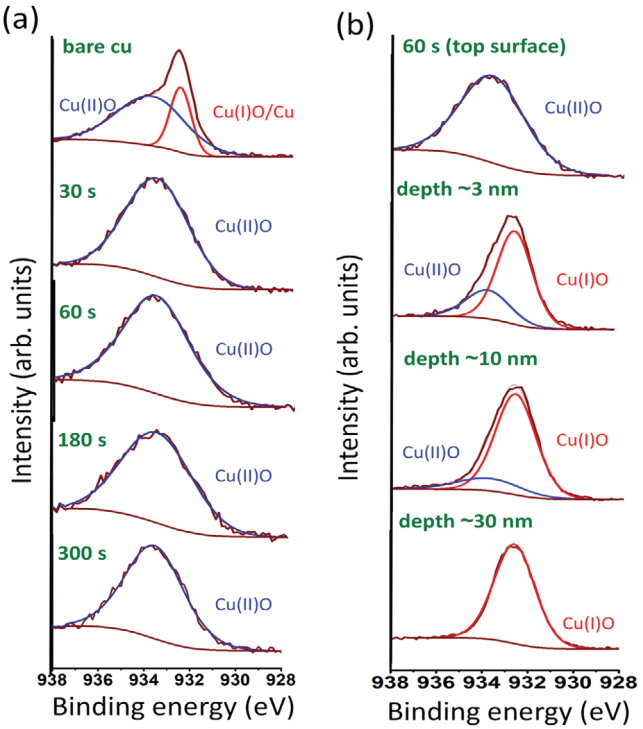

Figure 6. a) X-ray photoelectron spectra of core level Cu 2p of the as-polished Cu electrode and plasma modified Cu electrodes in 0.01 M KOH + 0.001 M SiO_2 at 525 V for 30, 60, 180, and 300 s. b) Depth profiling spectra of plasma modified Cu electrode (525 V, 60 s) recorded at 3, 10, and 30 nm min^{-1} Ar^+ sputtering. The spectra are fitted with a linear combination of the corresponding Cu, Cu_2O, and CuO reference spectra.

Figure 6b.[71] Interestingly, the intensity of the Cu(II)O peak significantly decreases accompanied by an increase of Cu(I)O as a function of sputtering depth. More importantly, Cu(II)O cannot be detected after 30 min. sputtering, in contrast, Cu(I)O is observed at 30 nm depth from the surface. Based on these XPS results, it can be concluded that the plasma-modified Cu electrodes comprise CuO as a thin outer layer (or shell) and a considerable amount of Cu_2O as an inner layer.

The atomic % of Cu, Si, and O of Cu electrodes after plasma electrolysis at 525 V in 0.01 M KOH + 0.001 M SiO_2 as a function of polarization times was determined by XPS analysis and the results are shown in Figure S5, Supporting Information. Notably, the values obtained by XPS are comparable to those detected by EDS (Figure S2, Supporting Information), indicating the reliability of both techniques.

2.4. Electrochemical Characterization

Afterward, structural changes of the Cu electrodes induced by the anodic plasma at 525 V in 0.01 M KOH and 0.01 M KOH + 0.001 M SiO_2 electrolytes as a function of processing time (30, 60, 120, 180, 300, and 600 s) were studied using cyclic voltammetry. The voltammograms of the Cu electrodes were recorded in 0.1 M KOH at a scan rate of s = 50 mV s^{-1}. **Figure 7**a,b shows the first cycle of the current–potential curves for as-polished and plasma-treated Cu electrodes in 0.01 M KOH and 0.01 M KOH + 0.001 M SiO_2, respectively. The first cycles were recorded after holding the potential at –0.2 V versus RHE until the lowest reduction current was observed. Furthermore, the current in these voltammetric profiles was normalized to the electrochemically active surface area (EASA). Asymmetrical oxidation and reduction peaks were observed for plasma-treated Cu electrodes in KOH and KOH + Si electrolytes at ≈0.05 V and 0.35 V versus RHE. The peaks of low intensity 0.05 V correspond to the adsorption and desorption of OH^- on Cu(111) terraces, while the pronounced peaks at 0.35 V were related to the oxidation and reduction of Cu to Cu(I)O on different domains of the polycrystalline Cu surfaces.[72,73] The absence of the oxidation and reduction peaks at ≈0.05 V versus RHE for the as-polished Cu electrodes indicates that the anodic plasma treatment induces the formation of Cu(111) sites. Additionally, the characteristic features of voltammograms recorded after anodic plasma treatment in 0.01 M KOH or 0.01 M KOH + 0.001 M SiO_2 electrolytes for different polarization times (from 30 to 600 s) are similar. However, the EASA ratios are significantly altering as a function of the different experimental conditions, including plasma treatment in either 0.01 M KOH or 0.01 M KOH + 0.001 M SiO_2 electrolytes (electrolyte compositions) and processing time, as presented in Figure 7c. The EASA has been determined by comparing the double–layer capacity of the plasma-treated and of as-polished Cu electrodes at –0.10 V versus RHE, where neither Faraday reactions nor adsorption processes occur.[31,74] Interestingly, the EASA ratios of Cu electrodes polarized in 0.01 M KOH or 0.01 M KOH + 0.001 M SiO_2 provide the same trends as a function of time, but one could notice substantial differences in the EASA as a function of the electrolyte composition. Figure 7c demonstrates that the EASA increases after plasma treatment in both electrolytes up to 180 s, and then it becomes almost steady until 600 s. Moreover, the EASA ratios drastically increase for plasma-treated Cu electrodes in 0.01 M KOH + 0.001 M SiO_2 (EASA factor 32–50) compared to the ones treated in only 0.01 M KOH (EASA factor 7–10) over the investigated processing time. These results can be explained by comparison to SEM. The SEM micrographs indicate that the presence of SiO_2 nanoparticles in the electrolyte results in the formation of coral-like microstructures, consequently, increasing the EASA. Furthermore, the coral-like microstructures are growing as a function of the treatment time until 300 s, after which the growth slows down. These findings highlight that the SEM analysis and electrochemical results are complementing each other.

2.5. Post Electrochemical Characterization and Formation of Nanospheres

After the electrochemical characterization, the surface morphology and chemical composition of the plasma-treated Cu electrodes were investigated by SEM and EDS. The electrochemical measurements were conducted by holding the potential at –0.2 V versus RHE until the lowest reduction current was detected, followed by cycling five times in the potential range between –0.2 and 0.4 V versus RHE. Remarkably, this electrochemical treatment induces a drastic structural transformation characterized by the formation of Cu nanospheres

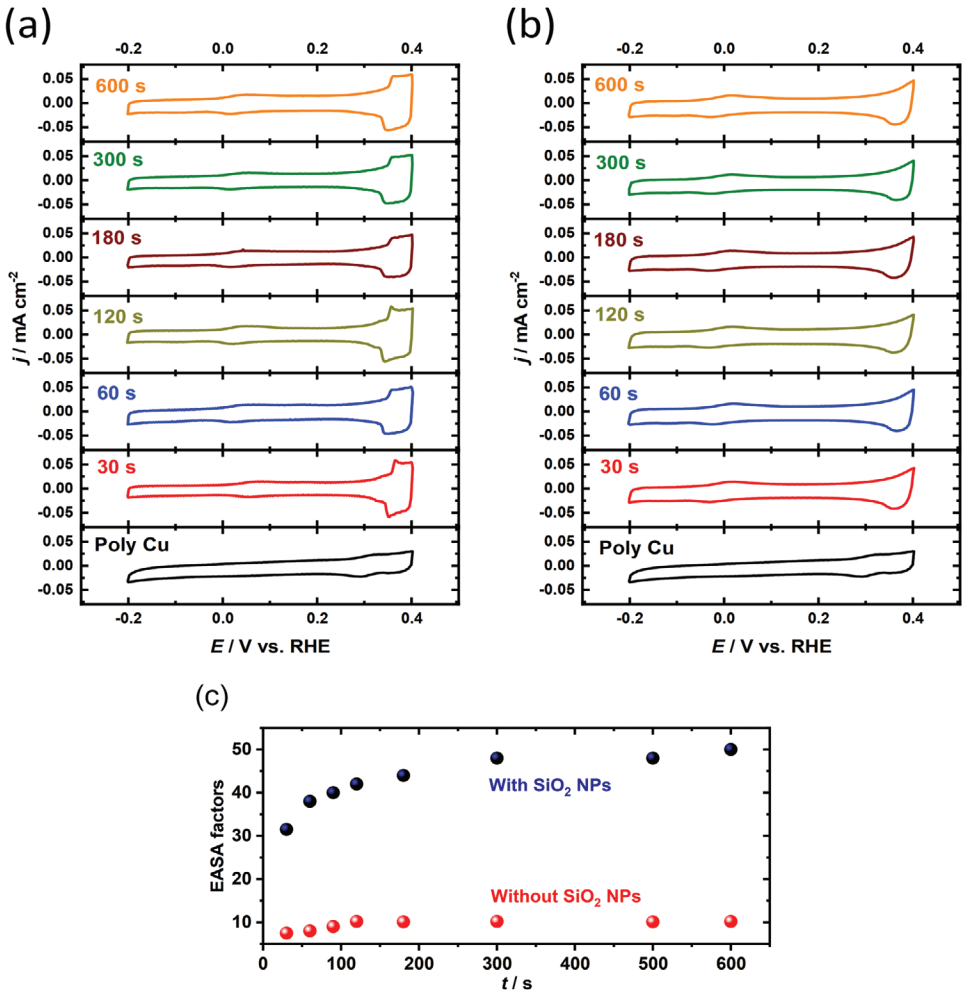

Figure 7. Cyclic voltammetry profiles of bare and plasma modified Cu electrodes in a) 0.01 M KOH electrolyte, and b) 0.01 M KOH + 0.001 M SiO_2 electrolyte at 525 V for different treatment times (30, 60, 120, 180, 300, and 600 s), which was recorded in 0.1 M KOH at 50 mV s^{-1}. c) Electrochemically active surface area factors as a function of treatment time for the Cu electrodes treated in 0.01 M KOH or 0.01 M KOH + 0.001 M SiO_2.

assembled into the coral-like microstructures, as shown in **Figure 8**a–d. After the formation of nanospheres, there were no further structure changes even after cycling more than 200 times in the aforementioned potential range indicating their high stability. These nanospheres are homogeneously distributed over the Cu surface with an average size of 150–200 nm. Such structure formation or transformation processes as a function of electrochemical treatment of metal electrodes are already known for different systems.[75,76] The EDS elemental mapping analysis reveals a significant reduction of O (8%) content and relative enrichment of Cu (88%) on the surface as a result of the electrochemical treatment compared to the freshly plasma-treated Cu electrode (Figure S6, Supporting Information). These structural transformations are observed for all samples that are plasma-treated at various processing times. Our results thus show that, by applying the aforementioned electrochemical treatment procedure, not only the surface morphology is altered, but also the chemical composition at the interface. Based on the EDS results obtained before and after electrochemical measurements, it seems that the reduction of the oxide layer plays a significant role in the fabrication of Cu microspheres. This could be an interesting strategy for a rapid two-step fabrication of nanostructured Cu electrodes by (i) producing microstructured electrodes using plasma treatment and then (ii) transforming the microstructures to nanostructures by simple electrochemical treatment.

To investigate the effect of the electrochemical treatment on the oxidation states of the plasma-modified Cu surface (525 V, 60 s), an XPS depth profiling analysis was performed with different sputter depth rates of 3, 10, and 30 nm min^{-1}, as shown in **Figure 9**. Remarkably, the oxidation state of Cu species of the topmost oxide layer of the plasma-treated Cu electrode was changed after the electrochemical treatment and formation of Cu nanospheres, as shown in Figures 6 and 9, respectively. The top surface of the Cu nanospheres was composed of a significant amount of Cu(I)O and a minor amount of Cu(II)O and $Cu(OH)_2$. The electrochemical treatment sustainably reduced the amount Cu(II)O due to the reduction step by holding the potential at –0.2 V versus RHE until the lowest reduction current was obtained. The appearance of $Cu(OH)_2$ only on the surface is attributed to surface OH adsorption on different low index surfaces during the electrochemical measurements. The

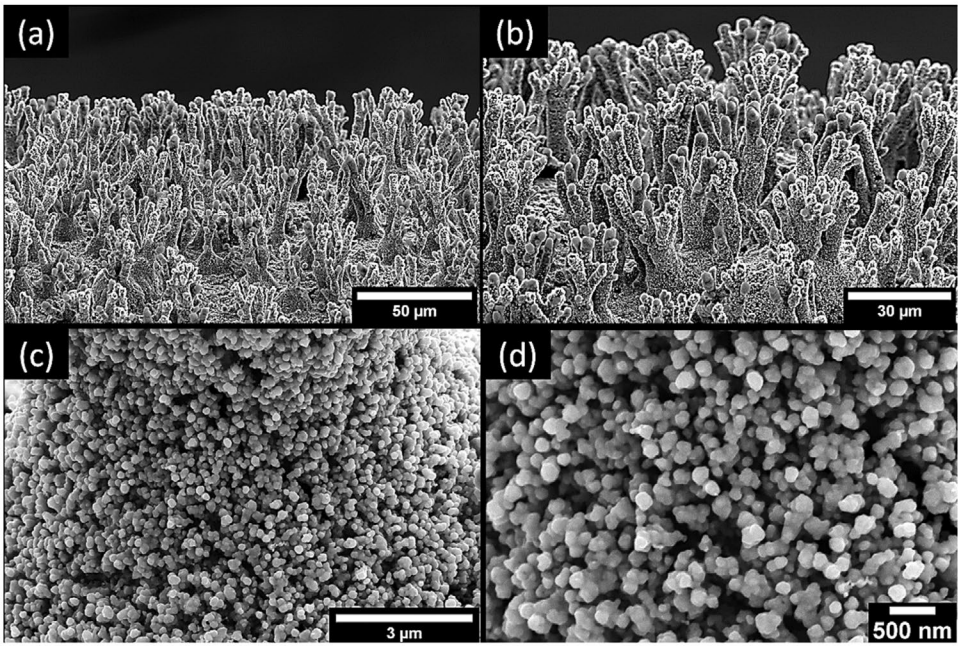

Figure 8. a–d) SEM images recorded at different magnifications for the coral-like structure after electrochemical measurements, which shows the formation of nanospheres over the coral surface.

intensity of the Cu(II)O peak considerably diminishes accompanied by an improvement of Cu(I)O with a further increase of sputtering depth. This trend is similar to that observed for the Cu electrodes before electrochemical treatment. These findings reveal that the electrochemical treatment influences the oxidation state of the Cu species of the top surface of the plasma-treated Cu electrodes.

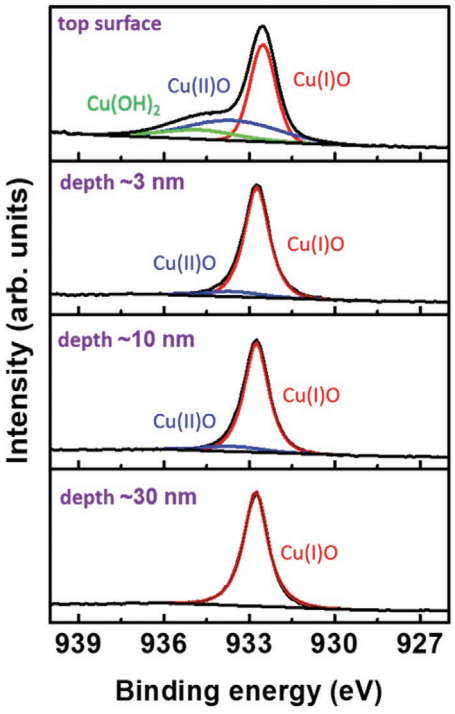

Figure 9. X-ray photoelectron depth profiling spectra of plasma-treated Cu electrode (525 V, 60 s) after the electrochemical treatment and formation of nanospheres. The spectra were recorded at 3, 10, and 30 nm min^{-1} Ar^+ sputtering.

2.6. Conversion Reactions of Plasma-Treated Cu Electrode with Lithium

The affinity of the plasma-modified Cu electrode compared to the untreated one toward Lithium (Li) has been investigated using Auger electron spectroscopy (AES) analysis. To reach this aim, Cu electrodes before and after the formation of 3D coral-like microstructures at 525 V for 60 s were cycled in 2.0 M LiOH electrolyte 25 times in the potential range between –0.80 and 0.80 V versus Ag/AgCl. The results are presented in Figure S7 and Table S1, Supporting Information, accompanied by further details. Remarkably, the plasma-treated Cu electrode shows a high affinity toward Li indicated by the presence of the reaction product Li_2O (see AES study in the Supporting Information).[77–79] This high affinity toward Li is due to the porous oxide structure obtained by plasma. Additionally, the Cu−O−SiO_x interface might play a role in such behavior.[57] In contrast, the surface of the as-received Cu electrode was covered by flake-like structures. These flake-like deposits had been analyzed by the AES. The conversion reaction of the smooth Cu electrode proceeded in a superficial layer which eventually peeled off the electrode surface, thus, limiting the ability of lithium to penetrate through the surface during electrochemical cycling. The deep incorporation of Li into the porous structure of the plasma-treated electrode indicated that such electrodes could be promising for lithium deposition in lithium-ion batteries.

3. Conclusion

In this study, we investigated the electrolysis of Cu electrodes in 0.01 M KOH and 0.01 M KOH + 0.001 M SiO_2 at a wide voltage range from 50 to 600 V. The electrolysis of Cu electrode in both electrolytes induces significant changes in surface structure, but one could observe substantial morphological differences as a function of the electrolyte composition. Interestingly, the presence of SiO_2 nanoparticles (11 nm) induces self-organization and self-assembly at the plasma/Cu interfaces resulting in the fabrication of homogenously distributed 3D coral-like microstructures. These microstructures were only detectable in the plasma regime (500–575 V), indicating the active incorporation of SiO_2 at sufficiently high voltages. High-energy discharges are required for melting the SiO_2 nanoparticles, consequently, they can react with the electrode surface. It seems that SiO_2 serves as a sacrificial nanoparticles template, resulting in the growth of 3D coral-like microstructures. These results indicate that the coral-like microstructures growth starts from the coral seeds that are homogenously distributed after electrolysis at 400 V. The thickness of the microstructured layer can be controlled over a wide range from 1–70 µm as a function of the plasma processing time. EDS analysis and elemental mapping reveal a high content of O and Cu, as well as a small amount of Si which is homogeneously distributed over the microstructures. Furthermore, XPS depth profiling measurements imply that the plasma-treated Cu electrodes comprise CuO as a thin outer layer and a substantial amount of Cu_2O as an inner layer. The surface structure of Cu electrodes before and after plasma electrolysis in 0.01 M KOH and 0.01 M KOH + 0.001 M SiO_2 at 525 V for various treatment times was characterized by cyclic voltammetry. The plasma treatment of Cu electrodes in both electrolytes induces the formation of Cu(111) sites accompanied by a remarkable increase in the EASA. Moreover, the EASA ratios drastically increase for plasma-treated Cu electrodes in 0.01 M KOH + 0.001 M SiO_2 (EASA factor 32–50) compared to the ones treated in only 0.01 M KOH (EASA factor 7–10) over the investigated processing time. The post electrochemical characterizations indicate that the reduction of the oxide layer during the electrochemical measurements drives a structural transformation to Cu nanospheres with an average size of 150–200 nm, but still assembled into the coral-like microstructures. The principles described here provide guidelines for engineering the Cu surfaces over a wide range of possibilities that might be promising to fabricate Cu electrodes of the desired surface structure for energy-related applications such as water splitting, CO_2 electrochemical reduction, and others. Furthermore, as a proof of concept regarding the applicability of the fabricated electrodes, preliminary results of the AES study indicate the high affinity of the plasma-treated electrodes toward Li intercalation, which is interesting for lithium-ion batteries.

4. Experimental Section

Plasma Experiments: Plasma electrolysis (PE) was conducted using a TDK-Lambda programmable DC power supply (GEN600-1.3/E, 1U, 780W, RS-232/RS-485). A LabVIEW software (National Instruments) was used to control the power supply and record the voltage and current data electronically. Electrolysis was carried out in a double-walled glass cell with a volume of 300 mL, equipped with magnetic stirring and a water-cooling system to maintain the electrolyte temperature in the range of 30–45 °C. Stainless steel with a dimension of 20 mm × 20 mm × 2 mm was used as a counter electrode (cathode), and a Cu wire (diameter 0.5 mm, 99.995+%, MaTecK, Jülich, Germany) served as the working electrode (anode). The Cu electrode was prepared by sonicating the Cu wire in 85% phosphoric acid (Merck) for 1 min to remove organic contaminants and the native oxide layer from the surface. The Cu wire was then thoroughly rinsed with ultra-pure water (18.2 MΩ cm, TOC ≤ 3 ppb) and dried in air before use. A polypropylene tip was used on both sides of the Cu wire to define the treatment area and obtain a homogenous electric field during electrolysis. The distance between the cathode and anode was maintained at 50 mm. Two types of alkaline electrolytes were used in the experiment, which contained 200 mL of 0.01 M KOH (99.99%, Sigma–Aldrich) and 200 mL of 0.01 M KOH + 0.001 M SiO_2 (particle size 11 nm, 99.8%, Sigma–Aldrich). Electrolyte solutions were prepared using ultra-pure water, and a magnetic stirrer was used to facilitate the uniform distribution of the particles in the electrolyte. After the experiment, the prepared electrodes were thoroughly rinsed with ultra-pure water and dried in an N_2 gas flow.

Characterization: Surface morphologies, cross-sections, chemical composition, as well as elemental mapping of the electrodes were analyzed using focused ion beam-scanning electron microscopy (FIB-SEM, Scios, Germany) coupled with energy dispersive spectroscopy (EDS, Ametek, USA). Imaging was performed using a secondary electron detector, while keeping the working distance at ≈10 mm, and operating at an accelerated voltage of 5 kV (surface information) and 20 kV (bulk information). For cross-section analyses via surface milling, gallium (Ga) ion beam source with a beam current of 1.5 nA (at 20 keV) was used. Before milling, the surface area of interest was deposited with a platinum strip to protect the top surface of the area from the ion beam.

The elemental composition and depth profiling of the sample surfaces were analyzed by X-ray photoelectron spectroscopy (XPS) measurements using monochromatized Al K_α (1486.6 eV) radiation (PHI 5800 MultiTechnique ESCA System, Physical Electronics) with a detection angle of 45°. A successive Argon ion (Ar^+) sputter treatment was carried out to get a depth profile of the chemical composition and oxidation states of the sample in the surface-near region. The topmost surface layers were removed by employing Ar^+ sputtering ($I_{Sp} \approx 1$ mA; $U_{Sp} = 5$ kV) with ≈1, 3, and 30 nm min^{-1}. To neutralize the surface charge, a low-energy electron flood gun (current, 3 µA) was used to deliver electrons to the sample surface. All binding energies were calibrated from the main carbon peak using the C_{1s} peak at 284.8 eV.

Auger electron spectroscopy (AES) measurements had been performed with a PHI 660 Scanning Auger Nanoprobe from Perkin Elmer Corp., Physical Electronics Division. As an electron gun and Auger electron analyser, a PHI 25–120 Electron Gun and Cylindrical Mirror Analyser from the same company were used. Since AES is a surface-sensitive method limited to the first three to five layers of the material, the samples had been measured in pristine, and after being sputtered for 70 s, which corresponds to an estimated depth of four to six further layers. Sputter experiments were conducted with argon ions of 0.5 µA sputter current, 150 s acquisition time, and 5.0 keV primary electron energy.

Electrochemical measurements were performed using a HEKA PG510 potentiostat. A conventional three-electrode glass cell was utilized for the characterization of the electrodes in 0.1 M KOH electrolyte using a HydroFlex RHE electrode (Gaskatel) as a reference electrode and a graphite rod as a counter electrode. Ultra-pure water (18.2 MΩ cm, TOC ≤ 3 ppb) was used for electrolyte preparation and apparatus cleaning. All chemicals were used as obtained without further purification. The electrolyte was deaerated with nitrogen, before and during the experiments. All electrochemical measurements in this study were carried out at room temperature (19–22 °C).

Supporting Information

Supporting Information is available from the Wiley Online Library or from the author.

Acknowledgements

This work was funded by the Deutsche Forschungsgemeinschaft (DFG, German Research Foundation) within the collaborative research center SFB-1316 as well as under Germany´s Excellence Strategy – EXC 2154 – Project number 390874152. The authors gratefully acknowledge Dr. Attila Farkas for the Auger Electron Spectroscopy (AES) measurement and data evaluation as well as Dr. Thomas Diemant for the XPS measurements. P. W. M. acknowledges support from the German Federal Ministry of Education and Research in the framework of the project Catlab (03EW0015A/B).

Open access funding enabled and organized by Projekt DEAL.

Conflict of Interest

The authors declare no conflict of interest.

Data Availability Statement

Research data are not shared.

Keywords

copper, micro/nanostructuring, plasma electrolysis, self-organization, silica nanoparticles

Received: July 20, 2021
Revised: October 1, 2021
Published online: October 27, 2021

[1] O. S. Bushuyev, P. de Luna, C. T. Dinh, L. Tao, G. Saur, J. van de Lagemaat, S. O. Kelley, E. H. Sargent, *Joule* **2018**, *2*, 825.
[2] P. De Luna, C. Hahn, D. Higgins, S. A. Jaffer, T. F. Jaramillo, E. H. Sargent, *Science* **2019**, *364*, eaav3506.
[3] M. J. Orella, Y. Román-Leshkov, F. R. Brushett, *Curr. Opin. Chem. Eng.* **2018**, *20*, 159.
[4] G. Giuffredi, T. Asset, Y. Liu, P. Atanassov, F. di Fonzo, *ACS Mater. Au* **2021**, *1*, 6.
[5] J. Linnemann, K. Kanokkanchana, K. Tschulik, *ACS Catal.* **2021**, *11*, 5318.
[6] C. Hahn, T. Hatsukade, Y. G. Kim, A. Vailionis, J. H. Baricuatro, D. C. Higgins, S. A. Nitopi, M. P. Soriaga, T. F. Jaramillo, *Proc. Natl. Acad. Sci. U.S.A.* **2017**, *114*, 5918.
[7] H. Xu, D. Rebollar, H. He, L. Chong, Y. Liu, C. Liu, C. J. Sun, T. Li, J. v. Muntean, R. E. Winans, D. J. Liu, T. Xu, *Nat. Energy* **2020**, *5*, 623.
[8] A. Sajeev, V. K. Mariappan, D. Kesavan, K. Krishnamoorthy, S.-J. Kim, *Mater. Adv.* **2021**, *2*, 455.
[9] Y. X. Lin, S. N. Zhang, Z. H. Xue, J. J. Zhang, H. Su, T. J. Zhao, G. Y. Zhai, X. H. Li, M. Antonietti, J. S. Chen, *Nat. Commun.* **2019**, *10*, 4380.
[10] Q. Zhu, X. Sun, D. Yang, J. Ma, X. Kang, L. Zheng, J. Zhang, Z. Wu, B. Han, *Nat. Commun.* **2019**, *10*, 3851.
[11] S. Nitopi, E. Bertheussen, S. B. Scott, X. Liu, A. K. Engstfeld, S. Horch, B. Seger, I. E. L. Stephens, K. Chan, C. Hahn, J. K. Nørskov, T. F. Jaramillo, I. Chorkendorff, *Chem. Rev.* **2019**, *119*, 7610.
[12] J. Yu, J. Wang, Y. Ma, J. Zhou, Y. Wang, P. Lu, J. Yin, R. Ye, Z. Zhu, Z. Fan, *Adv. Funct. Mater.* **2021**, *31*, 2102151.
[13] T. Ilyas, F. Raziq, S. Ali, A. Zada, N. Ilyas, R. Shaha, Y. Wang, L. Qiao, *Mater. Des.* **2021**, *204*, 109674.
[14] B. Chakraborty, R. Beltrán-Suito, V. Hlukhyy, J. Schmidt, P. W. Menezes, M. Driess, *ChemSusChem* **2020**, *13*, 3222.
[15] C. Panda, P. W. Menezes, M. Zheng, S. Orthmann, M. Driess, *ACS Energy Lett.* **2019**, *4*, 747.
[16] K. Jiang, Y. Huang, G. Zeng, F. M. Toma, W. A. Goddard, A. T. Bell, *ACS Energy Lett.* **2020**, *5*, 1206.
[17] Y. Huang, A. D. Handoko, P. Hirunsit, B. S. Yeo, *ACS Catal.* **2017**, *7*, 1749.
[18] C. W. Li, M. W. Kanan, *J. Am. Chem. Soc.* **2012**, *134*, 7231.
[19] P. Wang, M. Qiao, Q. Shao, Y. Pi, X. Zhu, Y. Li, X. Huang, *Nat. Commun.* **2018**, *9*, 4933.
[20] A. Eilert, F. Cavalca, F. S. Roberts, J. Osterwalder, C. Liu, M. Favaro, E. J. Crumlin, H. Ogasawara, D. Friebel, L. G. M. Pettersson, A. Nilsson, *J. Phys. Chem. Lett.* **2017**, *8*, 285.
[21] S. Jiao, X. Fu, L. Zhang, L. Zhang, S. Ruan, Y. J. Zeng, H. Huang, *Nano Today* **2021**, *36*, 101028.
[22] A. Rajput, A. Kundu, B. Chakraborty, *ChemElectroChem* **2021**, *8*, 1698.
[23] D. Giziński, A. Brudzisz, J. S. Santos, F. Trivinho-Strixino, W. J. Stępniowski, T. Czujko, *Catalysts* **2020**, *10*, 1338.
[24] A. N. Kuhn, H. Zhao, U. O. Nwabara, X. Lu, M. Liu, Y. T. Pan, W. Zhu, P. J. A. Kenis, H. Yang, *Adv. Funct. Mater.* **2021**, *31*, 2101668.
[25] D. Gao, I. Zegkinoglou, N. J. Divins, F. Scholten, I. Sinev, P. Grosse, B. R. Cuenya, *ACS Nano* **2017**, *11*, 4825.
[26] L. Gao, C. Pang, D. He, L. Shen, A. Gupta, N. Bao, *Sci. Rep.* **2015**, *5*, 16061.
[27] M. Biçer, I. Şişman, *Powder Technol.* **2010**, *198*, 279.
[28] V. Mantella, S. B. Varandili, J. R. Pankhurst, R. Buonsanti, *Chem. Mater.* **2020**, *32*, 9780.
[29] S. Popović, M. Smiljanić, P. Jovanovič, J. Vavra, R. Buonsanti, N. Hodnik, *Angew. Chem., Int. Ed.* **2020**, *59*, 14736.
[30] A. Kaliyaraj Selva Kumar, Y. Zhang, D. Li, R. G. Compton, *Electrochem. Commun.* **2020**, *121*, 106867.
[31] M. M. Elnagar, J. M. Hermann, T. Jacob, L. A. Kibler, *Electrochim. Acta* **2021**, *372*, 137867.
[32] M. M. Elnagar, J. M. Hermann, T. Jacob, L. A. Kibler, *Curr. Opin. Electrochem.* **2021**, *27*, 100696.
[33] C. Rurainsky, A. G. Manjón, F. Hiege, Y. T. Chen, C. Scheu, K. Tschulik, *J. Mater. Chem. A* **2020**, *8*, 19405.
[34] P. Grosse, A. Yoon, C. Rettenmaier, S. W. Chee, B. R. Cuenya, *J. Phys. Chem. C* **2020**, *124*, 26908.
[35] D. He, G. Wang, G. Liu, H. Suo, C. Zhao, *Dalton Trans.* **2017**, *46*, 3318.
[36] A. Altaweel, T. Gries, S. Migot, P. Boulet, A. Mézin, T. Belmonte, *Surf. Coat. Technol.* **2016**, *305*, 254.
[37] I. Levchenko, I. I. Beilis, M. Keidar, *Adv. Mater. Technol.* **2016**, *1*, 1600008.
[38] B. Gong, X. Zhao, Z. Pan, S. Li, X. Wang, Y. Zhao, C. Luo, *Sci. Rep.* **2014**, *4*, 4713.
[39] O. Baranov, I. Levchenko, J. M. Bell, J. W. M. Lim, S. Huang, L. Xu, B. Wang, D. U. B. Aussems, S. Xu, K. Bazaka, *Mater. Horiz.* **2018**, *5*, 765.
[40] S. Chauhan, T. Barman, M. Bhatnagar, M. Ranjan, S. Mukherjee, *Rev. Sci. Instrum.* **2017**, *88*, 063507.
[41] W. Zhu, P. Niraula, P. G. C. Almeida, M. S. Benilov, D. F. N. Santos, *Plasma Sources Sci. Technol.* **2014**, *23*, 054012.
[42] C. Dai, D. Joung, J.-H. Cho, *Nano-Micro Lett.* **2017**, *9*, 27.
[43] C. Zhao, W. Zha, R. Cai, X. Nie, J. Tjong, *ACS Sustainable Chem. Eng.* **2019**, *7*, 5524.
[44] J. Hieda, N. Saito, O. Takai, *J. Vac. Sci. Technol., A* **2008**, *26*, 854.
[45] D. B. Padmanaban, R. McGlynn, E. Byrne, T. Velusamy, M. Swadźba-Kwaśny, P. Maguire, D. Mariotti, *Green Chem.* **2021**, *23*, 3983.
[46] X. Lu, C. Blawert, M. Mohedano, N. Scharnagl, M. L. Zheludkevich, K. U. Kainer, *Surf. Coat. Technol.* **2016**, *289*, 179.
[47] D.-W. Kim, B. Lee, D.-W. Park, *J. Electrochem. Soc.* **2019**, *166*, C3200.
[48] T. Li, X. Nie, *ACS Appl. Mater. Interfaces* **2018**, *10*, 16943.

[49] X. Lu, C. Blawert, M. L. Zheludkevich, K. U. Kainer, *Corros. Sci.* **2015**, *101*, 201.
[50] X. Lu, C. Blawert, Y. Huang, H. Ovri, M. L. Zheludkevich, K. U. Kainer, *Electrochim. Acta* **2016**, *187*, 20.
[51] B. S. Lou, Y. Y. Lin, C. M. Tseng, Y. C. Lu, J. G. Duh, J. W. Lee, *Surf. Coat. Technol.* **2017**, *332*, 358.
[52] A. Fattah-alhosseini, R. Chaharmahali, K. Babaei, *J. Magnesium Alloys* **2020**, *8*, 799.
[53] E. Nikoomanzari, A. Fattah-alhosseini, M. R. Pajohi Alamoti, M. K. Keshavarz, *Ceram. Int.* **2020**, *46*, 13114.
[54] C. Xu, G. Chen, Y. Zhao, P. Liu, X. Duan, L. Gu, G. Fu, Y. Yuan, N. Zheng, *Nat. Commun.* **2018**, *9*, 3367.
[55] J. J. Navarro, S. Tosoni, J. P. Bruce, L. Chaves, M. Heyde, G. Pacchioni, B. R. Cuenya, *J. Phys. Chem. C* **2020**, *124*, 20942.
[56] Y. Yamada, C.-K. Tsung, W. Huang, Z. Huo, S. E. Habas, T. Soejima, C. E. Aliaga, G. A. Somorjai, P. Yang, *Nat. Chem.* **2011**, *3*, 372.
[57] J. K. Ha, A. K. Haridas, G. B. Cho, H. J. Ahn, J. H. Ahn, K. K. Cho, *Appl. Surf. Sci.* **2019**, *481*, 307.
[58] G. Saito, S. Hosokai, M. Tsubota, T. Akiyama, *J. Appl. Phys.* **2011**, *110*, 023302.
[59] L. Zhu, Y. Li, W. Li, *Surf. Coat. Technol.* **2008**, *202*, 5853.
[60] D. G. Gregory, Q. Guo, L. Lu, C. J. Kiely, M. A. Snyder, *Langmuir* **2017**, *33*, 6601.
[61] G. B. Alteri, M. Bonomo, F. Decker, D. Dini, *Catalysts* **2020**, *10*, 1104.
[62] C. Zhao, W. Zha, R. Cai, X. Nie, J. Tjong, *ACS Sustainable Chem. Eng.* **2019**, *7*, 5524.
[63] C. Quan, Y. He, *Appl. Surf. Sci.* **2015**, *353*, 1320.
[64] M. M. Krishtal, P. V. Ivashin, A. V. Polunin, E. D. Borgardt, *Mater. Lett.* **2019**, *241*, 119.
[65] E. Artmann, P. V. Menezes, L. Forschner, M. M. Elnagar, L. A. Kibler, T. Jacob, A. K. Engstfeld, *ChemPhysChem* **2021**, https://doi.org/10.1002/cphc.202100433.
[66] P. Gupta, G. Tenhundfeld, E. O. Daigle, D. Ryabkov, *Surf. Coat. Technol.* **2007**, *201*, 8746.
[67] S. Sikdar, P. V. Menezes, R. Maccione, T. Jacob, P. L. Menezes, *Nanomaterials* **2021**, *11*, 1375.
[68] P. N. Belkin, S. A. Kusmanov, E. V. Parfenov, *Appl. Surf. Sci. Adv.* **2020**, *1*, 100016.
[69] P. Jiang, D. Prendergast, F. Borondics, S. Porsgaard, L. Giovanetti, E. Pach, J. Newberg, H. Bluhm, F. Besenbacher, M. Salmeron, *J. Chem. Phys.* **2013**, *138*, 024704.
[70] S. Poulston, P. M. Parlett, P. Stone, M. Bowker, *Surf. Interface Anal.* **1996**, *24*, 811.
[71] E. J. Broadhead, A. Monroe, K. M. Tibbetts, *Langmuir* **2021**, *37*, 3740.
[72] A. Bagger, R. M. Arán-Ais, J. H. Stenlid, E. Campos dos Santos, L. Arnarson, K. D. Jensen, M. Escudero-Escribano, B. Roldan-Cuenya, J. Rossmeisl, *ChemPhysChem* **2019**, *20*, 3096.
[73] A. Tiwari, H. H. Heenen, A. S. Bjørnlund, T. Maagaard, E. Cho, I. Chorkendorff, H. H. Kristoffersen, K. Chan, S. Horch, *J. Phys. Chem. Lett.* **2020**, *11*, 1450.
[74] H. Mistry, A. S. Varela, C. S. Bonifacio, I. Zegkinoglou, I. Sinev, Y. W. Choi, K. Kisslinger, E. A. Stach, J. C. Yang, P. Strasser, B. R. Cuenya, *Nat. Commun.* **2016**, *7*, 12123.
[75] P. Ahrens, M. Zander, U. Hasse, H. Wulff, C. Jeyabharathi, A. Kruth, F. Scholz, *ChemElectroChem* **2018**, *5*, 943.
[76] C. Köntje, G. Jerkiewicz, *Langmuir* **2013**, *29*, 10272.
[77] S. Patat, D. Blunt, A. Chippindale, P. Dickens, *Solid State Ionics* **1991**, *46*, 325.
[78] Y. Arachi, T. Setsu, T. Ide, K. Hinoshita, Y. Nakata, *Solid State Ionics* **2012**, *225*, 611.
[79] F. Klein, R. Pinedo, P. Hering, A. Polity, J. Janek, P. Adelhelm, *J. Phys. Chem. C* **2016**, *120*, 1400.